Study of the Sedov-Taylor Blast Wave Problem

Mario Veca

5 April 2018
(Translated: 1 February 2025)

Abstract

This study explores the Sedov-Taylor blast wave problem by numerically solving the governing differential equations in a polytropic gas. Using a fourth-order Runge-Kutta integration method, we analyze the evolution of self-similar profiles for density, pressure, velocity, and temperature. Additionally, we investigate the role of the stiffness parameter γ and its impact on the shockwave structure, highlighting key physical and computational insights.

Contents

1 Problem Formulation and Differential Equation Setup

We aim to use the equations of fluid dynamics to determine the behavior of state variables within the post-shock region of a violent explosion. To this end, we consider an explosion in a non-viscous polytropic fluid, where the propagation is described by a spherical shock front. From dimensional analysis, we can immediately conclude that the time-dependent distance of the shock front from the explosion center follows:

$$R_s(t) = k\left(\frac{Et^2}{\rho}\right)^{\frac{1}{5}} , \tag{1}$$

where E represents the energy released in the explosion, ρ is the medium density, and t is the time, with k being a dimensionless constant to be determined. From this formula, it follows that the shock wave velocity is given by:

$$V_s = \frac{d(R_s(t))}{dt} = \frac{2R_s(t)}{5t} , \tag{2}$$

which decreases as the expansion progresses.
In the shock-comoving reference frame, we can apply the jump conditions in the strong shock limit:

$$\frac{\rho_2}{\rho_1} = \frac{(\gamma+1){M_1}^2}{(\gamma-1){M_1}^2+2} \approx \frac{\gamma+1}{\gamma-1} , \tag{3}$$

$$\frac{v_2}{v_1} = \frac{(\gamma-1){M_1}^2+2}{(\gamma+1){M_1}^2} \approx \frac{\gamma-1}{\gamma+1} , \tag{4}$$

$$\frac{p_2}{p_1} = \frac{2\gamma{M_1}^2}{\gamma+1} - \frac{\gamma-1}{\gamma+1} \approx \frac{2\gamma{M_1}^2}{\gamma+1} , \tag{5}$$

where subscript 1 refers to the pre-shock state and subscript 2 refers to the post-shock state.
In the lab reference frame, the second equation transforms into[1]:

$$v_2' = V_s\frac{2}{\gamma+1} , \tag{6}$$

where we made the approximation $v_1' \ll V_s$. Furthermore, recalling that the sound speed satisfies the relation

$$c_s^2 = \frac{\gamma p}{\rho} . \tag{7}$$

[1]From now on, the prime notation will be omitted, as we will always refer to the fixed reference frame.

We can rewrite the post-shock density, velocity, and pressure in terms of the external medium properties:

$$\rho_2 = \rho \frac{\gamma+1}{\gamma-1} \ , \tag{8}$$

$$v_2 = V_s \frac{2}{\gamma+1} \ , \tag{9}$$

$$p_2 = \frac{2\rho {V_s}^2}{\gamma+1} \ . \tag{10}$$

Thus, the internal profiles of density, velocity, and pressure within the shock region must be determined by solving the fluid dynamics equations, with the boundary conditions given by the equations above. We introduce the self-similar variables:

$$\xi = \frac{r}{R_s} \ , \quad H(\xi) = \frac{\rho}{\rho_2} \ , \quad V(\xi) = \frac{v}{v_2} \ , \quad P(\xi) = \frac{p}{p_2} \ , \tag{11}$$

which satisfy $0 < \xi < 1$ with boundary conditions:

$$H(1) = V(1) = P(1) = 1 \ . \tag{12}$$

The fluid dynamics equations are the continuity equation, Euler's equation, and the adiabatic equation, where we recall that the entropy of a polytropic gas satisfies:

$$S = a \log\left(\frac{p}{\rho^\gamma}\right) \ , \tag{13}$$

$$\frac{\partial \rho}{\partial t} + \frac{1}{r^2}\frac{\partial (r^2 \rho v_r)}{\partial r} = 0 \ , \tag{14}$$

$$\frac{\partial v_r}{\partial t} + v_r \frac{\partial v_r}{\partial r} = -\frac{1}{\rho}\frac{\partial p}{\partial r} \ , \tag{15}$$

$$a\left(\frac{\partial}{\partial t} + v_r \frac{\partial}{\partial r}\right) \log\left(\frac{p}{\rho^\gamma}\right) = 0 \ . \tag{16}$$

By substituting, we obtain the following system of first-order nonlinear differential equations with non-constant coefficients. The reason why the system reduces from partial differential equations to ordinary differential equations is precisely due to the introduction of self-similar variables, which allow both time and spatial derivatives to be rewritten in terms of derivatives with respect to ξ:

$$-\xi H' + \frac{2}{\gamma+1}\left(H'V + HV'\right) + \frac{4}{\gamma+1}\left(\frac{HV}{\xi}\right) = 0 \ , \tag{17}$$

$$-2\xi V' - 3V + \frac{4VV'}{\gamma+1} + \frac{\gamma-1}{\gamma+1}\frac{2P'}{H} = 0 \ , \tag{18}$$

$$-3 - \frac{P'}{P}\xi + \frac{2}{\gamma+1}V\frac{P'}{P} + \gamma\xi\frac{H'}{H} - \frac{2\gamma}{\gamma+1}V\frac{H'}{H} = 0 \ , \tag{19}$$

with boundary conditions:

$$H(1) = P(1) = V(1) = 1 \ . \tag{20}$$

2 Integration of the System of Differential Equations

The system of differential equations can be solved numerically by rewriting it in normal form and using the fourth-order Runge-Kutta algorithm. This algorithm was chosen because, being of fourth order, it allows for a rapid reduction of numerical error as the integration step size decreases. The downside is that the execution of the numerical integration is slower. However, this computational cost is not significant for this problem, since the system does not contain a large number of equations, and the required number of integration steps is not excessively high (nor can it be, to avoid significant approximation errors due to computational precision limits). As a result, computational times remain short.
The numerical integration is performed by executing the C++ code attached. Figure 1 shows an example of the computed solutions for the functions $H(\xi)$, $P(\xi)$, and $V(\xi)$, considering a monoatomic gas with 3 degrees of freedom and an integration step size of $d\xi = 0.001$. The plot shows that the velocity profile exhibits a linear increase in the innermost region of the sphere, while it grows more steeply near the shock front. This result indicates that particles near the surface are dragged at a velocity comparable to that of the shock front. Over time, after the passage of the explosive shock, the fluid velocity decreases, but the relaxation process is gradual rather than instantaneous.
The pressure profile also exhibits an increasing trend but grows very slowly in the innermost part of the explosion and much more rapidly near the surface. This is consistent with the intuitive idea that most of the pressure-driven effects are concentrated in the region adjacent to the shock front.
Finally, the density profile shows a nearly constant value in the central region of the explosion, followed by a sharp increase near the shock front. This result aligns with the expectation that the explosion pushes most of the mass outward. It is also consistent with the pressure profile, as the motion of high-velocity particles has a pushing effect, and with the velocity profile, since higher velocities in the outer region correspond to greater mass transport.

Through numerical integration, it is also possible to determine the proportionality constant appearing in the expression for $R_s(t)$. From energy con-

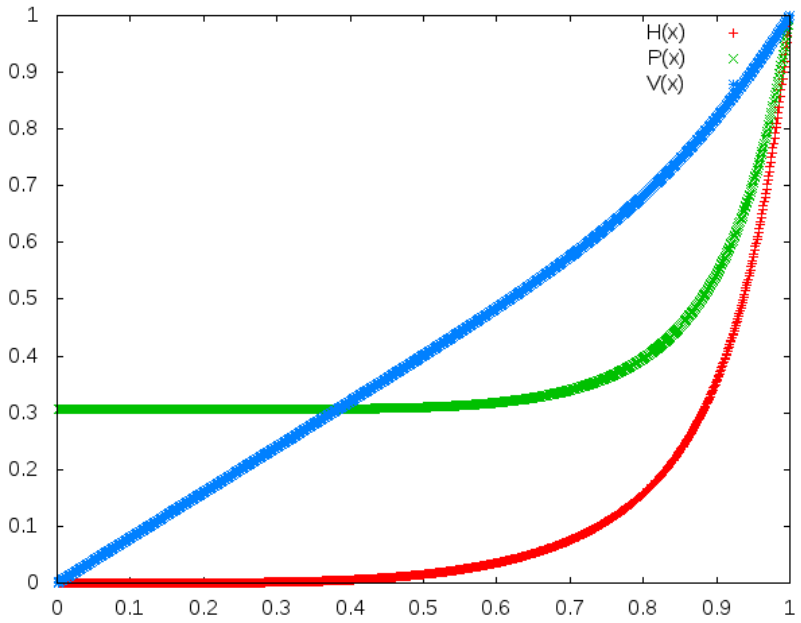

Figure 1: Graphs of the self-similar quantities of the problem. The red curve represents the density profile, the green curve represents the pressure profile, and the blue curve represents the radial velocity profile.

servation, we obtain:

$$E = \int_0^{R_s(t)} \rho \left(\frac{1}{2} v^2 + u \right) 4\pi r^2 dr \ , \tag{21}$$

where the internal energy is given by $u = \dfrac{p}{\rho\gamma}$. By substituting the expressions for ρ, p, v, and r in terms of the self-similar variables, we obtain:

$$k = \left(\frac{25(\gamma^2 - 1)}{32\pi I(\gamma)} \right)^{\frac{1}{5}} \ , \tag{22}$$

where

$$I(\gamma) = \int_0^1 (HV^2 + P)\xi^2 d\xi \ . \tag{23}$$

For the given numerical values, the result is $k = 1.152$.

By solving the system, it is also possible to determine the temperature profile in terms of the self-similar variable:

$$T(\xi) = \frac{T}{T_2} = \frac{P\rho_2}{P_2\rho} = \frac{P(\xi)}{H(\xi)} \ . \tag{24}$$

Figure 2 shows the computed temperature profile inside the shocked region. It is immediately apparent that the temperature diverges at the origin, meaning that the innermost regions of the gas experience the highest thermal agitation.

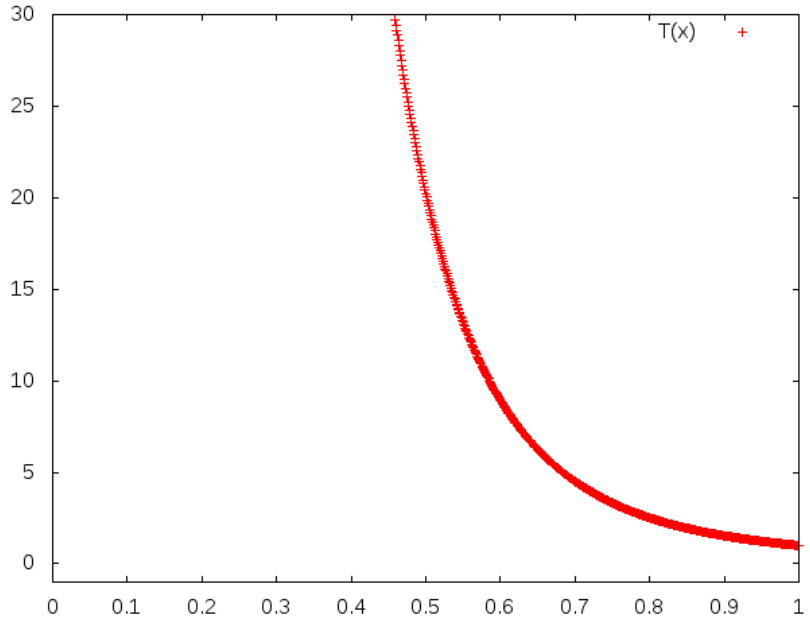

Figure 2: Graph of the self-similar temperature variable. The curve diverges at the origin, so only a finite portion is displayed.

Two observations can be made here: the first is that, even though the temperature diverges, this does not imply an infinite energy density, since the density simultaneously approaches zero. The second is that velocity, in contrast, increases as one moves away from the center of the sphere. This observation is consistent with the Second Law of Thermodynamics, as it shows that the passage of the shock wave transforms ordered radial motion into random thermal agitation.

3 Analysis as a function of γ

We aim to analyze how the solution changes as a function of the stiffness parameter, defined as $\gamma = \dfrac{2 + n_g}{n_g}$. Figures 3, 4, 5, and 6 show the self-similar profiles of density, pressure, velocity, and temperature inside the sphere for gases composed of molecules with 3, 5, and 7 degrees of freedom.

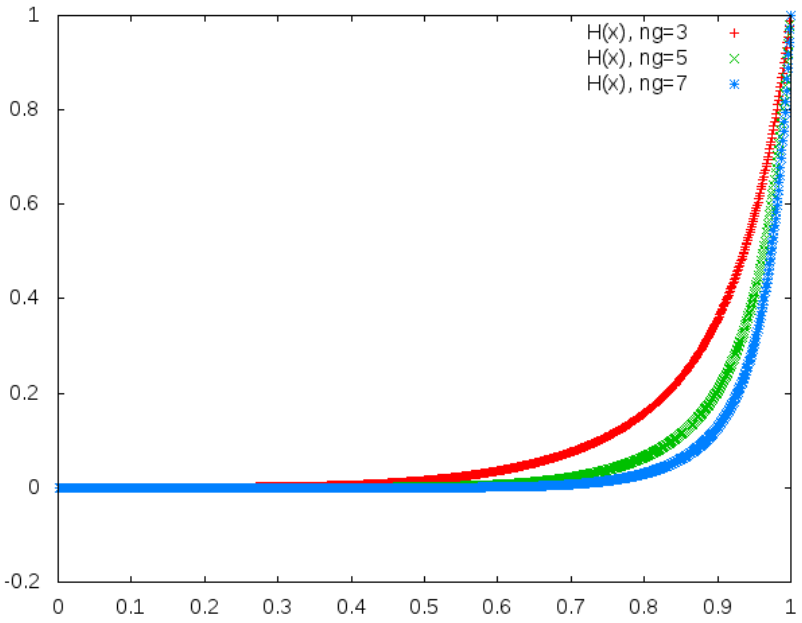

Figure 3: Self-similar density profiles. The red curve represents the profile for a gas with molecules having three degrees of freedom, the green curve corresponds to five degrees of freedom, and the blue curve represents seven degrees of freedom.

From the plots, we observe that increasing the number of degrees of freedom leads to greater mass accumulation near the discontinuity surface, while the pressure increases in the inner region of the explosion but remains concentrated immediately behind the shock front. The velocity profile tends to exhibit a more uniform increase, whereas the temperature diverges more significantly. These results align with the expectation that a greater distribution of energy among multiple degrees of freedom follows from the Second Law of Thermodynamics.
Additionally, we can compute the dimensionless constant k appearing in the formula for $R_s(t)$ as a function of γ, for the cases of 3, 5, and 7 degrees of freedom. The results obtained are:

$$k_3 = 1.152 \ , \quad k_5 = 1.033 \ , \quad k_7 = 0.964 \ . \tag{25}$$

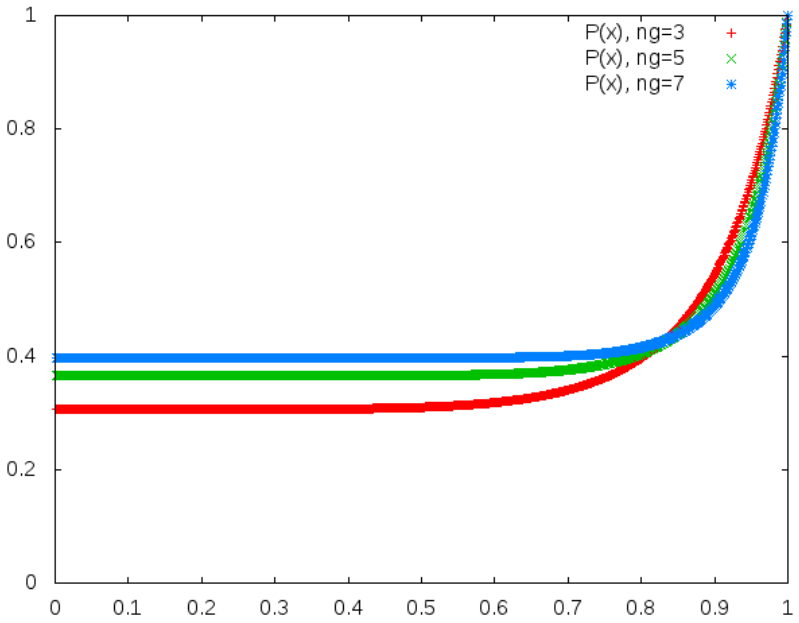

Figure 4: Self-similar pressure profiles. The red curve represents the profile for a gas with molecules having three degrees of freedom, the green curve corresponds to five degrees of freedom, and the blue curve represents seven degrees of freedom.

We observe that as the number of degrees of freedom increases, the value of k continues to decrease. This result is reasonable since k is proportional to the sphere's size at a given time. Since a larger γ corresponds to a stiffer medium, the shock wave propagates at a higher velocity. Equivalently, we observe that molecules with a higher number of degrees of freedom slow down the explosive shock because the energy is distributed over multiple degrees of freedom.

4 Observations on Numerical Integration Errors

In all previous analyses, we studied the problem and understood the behavior of the state functions without needing to consider the extreme case of a very high number of degrees of freedom, which is uncommon for most gases encountered in practice. However, as an instructive exercise in numerical integration and differential equation systems, we investigate what happens in this limit.
Figure 7 shows the behavior of the three variables $H(\xi)$, $P(\xi)$, and $V(\xi)$ in the case of 60 degrees of freedom.

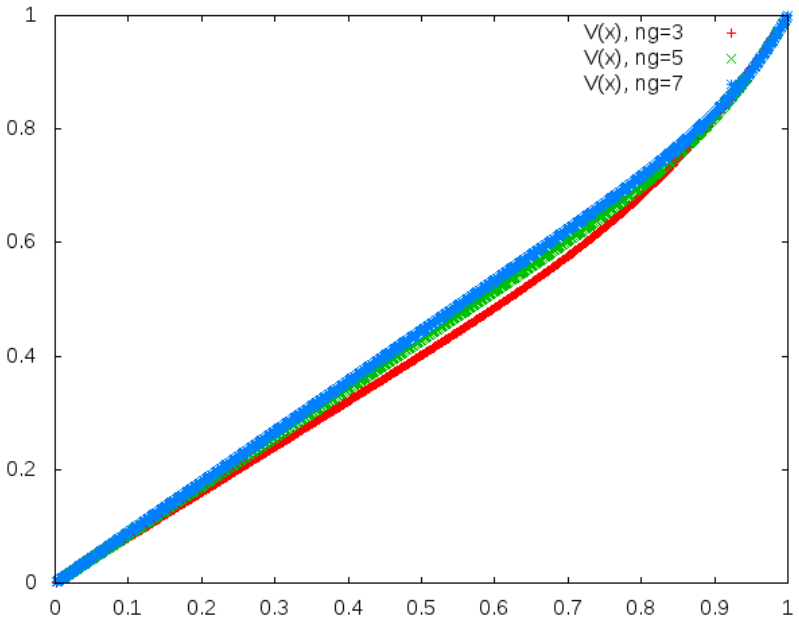

Figure 5: Self-similar velocity profiles. The red curve represents the profile for a gas with molecules having three degrees of freedom, the green curve corresponds to five degrees of freedom, and the blue curve represents seven degrees of freedom.

The plot clearly shows a divergence near the origin for the function $V(\xi)$. This can be understood by noting that in the limit where $\gamma \approx 1$ (here, $\gamma = 1.03$), the system of differential equations enters a regime of critical instability due to numerical integration errors. This occurs because one of the system's terms, specifically the term in the second equation that multiplies P', tends to vanish. As a result, the denominator in the expression for V' rapidly approaches zero, meaning that even a small integration error can cause a catastrophic increase in $V(\xi)$.

To demonstrate this, we repeat the numerical integration using the same number of degrees of freedom per particle, but this time using a smaller integration step size to sufficiently reduce numerical errors and eliminate their significant impact on the solution. Figure 8 confirms that by reducing the integration error, a stable solution is recovered.

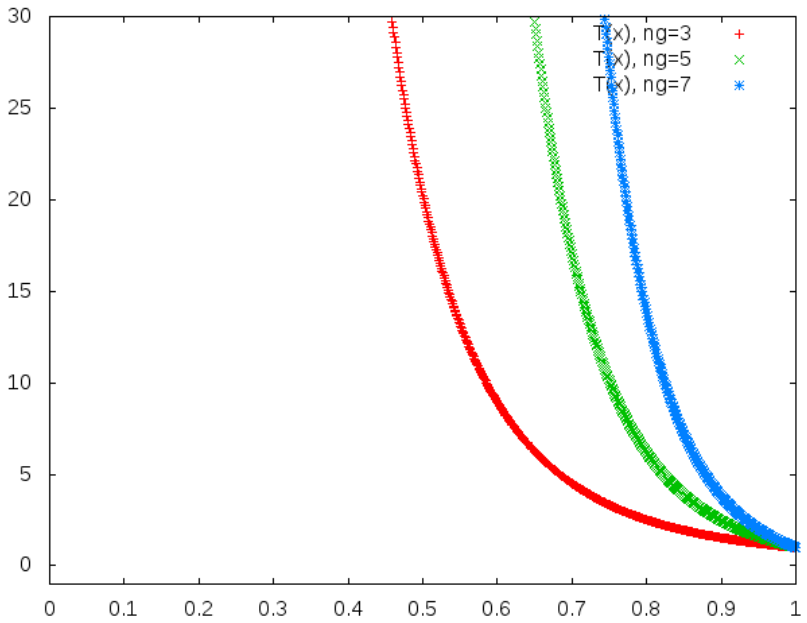

Figure 6: Self-similar temperature profiles. The red curve represents the profile for a gas with molecules having three degrees of freedom, the green curve corresponds to five degrees of freedom, and the blue curve represents seven degrees of freedom.

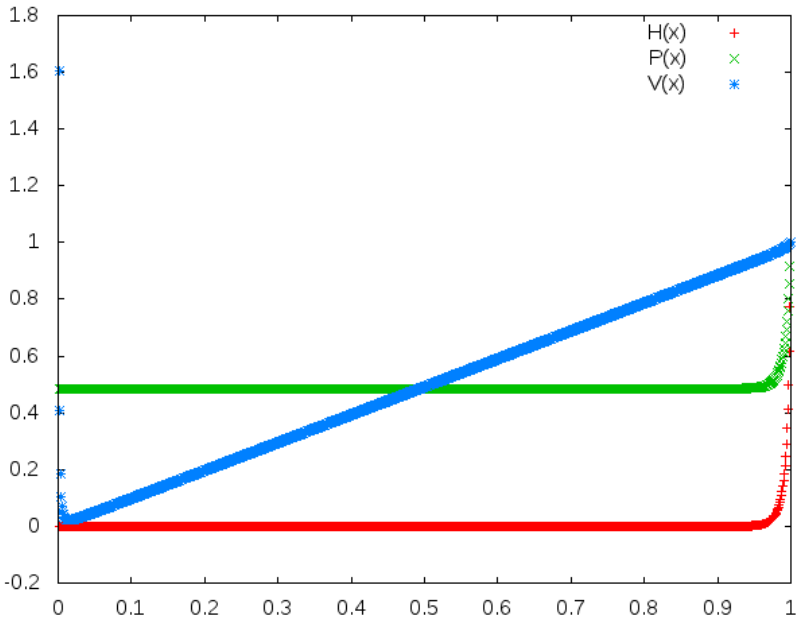

Figure 7: Self-similar profiles of the problem. The red curve represents the density profile, the green curve represents the pressure profile, and the blue curve represents the radial velocity profile. The numerical integration was performed with $n_{gradi} = 60$ and $d\xi = 0.001$.

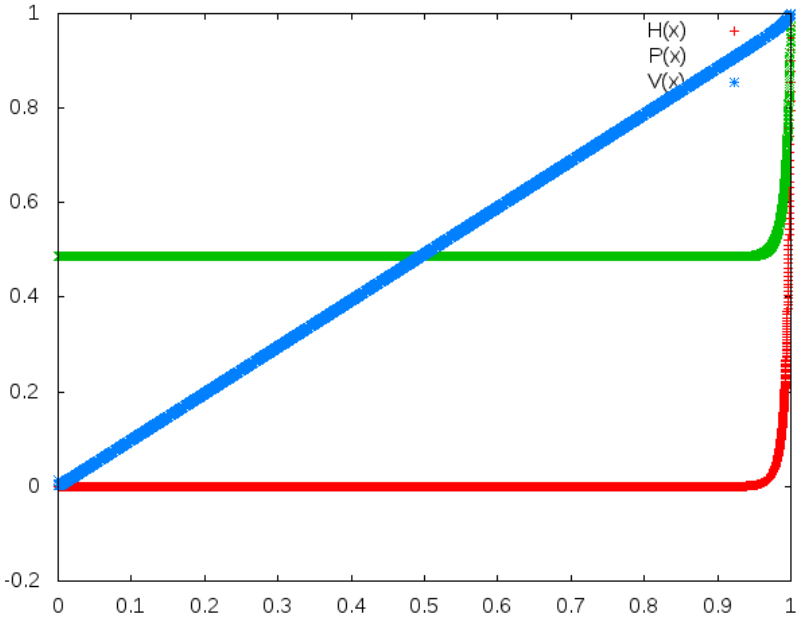

Figure 8: Self-similar profiles of the problem. The red curve represents the density profile, the green curve represents the pressure profile, and the blue curve represents the radial velocity profile. The numerical integration was performed with $n_{gradi} = 60$ and $d\xi = 0.0001$.